



21st European Conference on Fracture, ECF21, 20-24 June 2016, Catania, Italy

## How microscopic stress and strain analysis can improve the understanding of the interplay between material properties and variable amplitude fatigue

M. Thielen<sup>a,\*</sup>, M. Marx<sup>a</sup>, M. Sheikh-Amiri<sup>b</sup>, C. Boller<sup>b</sup>, C. Motz<sup>a</sup>

<sup>a</sup>Materials Science and Methods, Campus D2.3, 66123 Saarbrücken, Germany

<sup>b</sup>Non-Destructive Testing and Quality Assurance, Am Markt Zeile 4, 66123 Saarbrücken, Germany

### Abstract

*Lightweight construction* is one of the most demanded technologies in many engineering systems. In order to guarantee the safety of the whole system, it is mandatory to improve models that describe and predict its behavior under load. Fatigue, the damaging of materials under cyclic loading, is the main phenomenon leading to failure in e.g. automobile and aerospace components. Cyclic loading during service does usually not happen with constant amplitudes, rather there are complex patterns of different load levels. High load variations in these patterns lead to deviations from the linear Paris behavior. Strong decelerations occur as consequence of a single increased tensile load, which is known as the overload effect. Nevertheless, this effect does not affect all materials the same, there are materials that show a strong overload sensitivity and others on which overloads only have a minor influence. Reasons for this can be seen in the interplay of the underlying mechanisms of the overload effect: plasticity induced crack closure and compressive residual stresses. While both effects lead to crack tip shielding and a reduction of stress intensity, crack closure delays the opening of the crack tip and thereby reduces the effective  $\Delta K$  range, whereas compressive residual stresses superimpose with crack tip stresses and thereby reduce  $K_{\max}$ . Possible reasons for differences in the sensitivity can be differences in the strain hardening, both in the static and in the dynamic case, as well as in changes of the sign of stresses (Bauschinger effect). Since crack propagation is driven by local stresses and strains, measurements to examine differences in them have to be performed on a microscopic scale.

We could show that by the combination of modern measurement techniques – magnetic Barkhausen noise and digital image correlation in scanning electron microscope – we were able to image, separate and evaluate the mechanisms of the overload effect quantitatively. The calibrated magnetic Barkhausen noise microscope allows us measurements of residual stresses with a spatial resolution of 10  $\mu\text{m}$ . From the digital image correlation results we could evaluate the crack tip driving forces namely the crack opening behavior, changes in the stress intensity  $K$  and in the strain energy release rate via the  $J$ -integral. Using a simple model based on these results, we were furthermore able to predict the crack growth behavior due to the overload effect. These

Copyright © 2016 The Authors. Published by Elsevier B.V. This is an open access article under the CC BY-NC-ND license (<http://creativecommons.org/licenses/by-nc-nd/4.0/>).

Peer-review under responsibility of the Scientific Committee of ECF21.

\* Corresponding author. Tel.: +49 681 302 5160; fax: +49 681 302 5015.

E-mail address: [m.thielen@matsci.uni-sb.de](mailto:m.thielen@matsci.uni-sb.de)

results will be used to extend crack growth models, while taking the interaction of materials' properties with the mentioned mechanisms into account. This should enable a physically based, improved lifetime prediction and material selection for certain load patterns.

© 2016 The Authors. Published by Elsevier B.V.  
Peer-review under responsibility of the Scientific Committee of ECF21.

*Keywords:* Fatigue Crack Growth; Overload Effect; Residual Stress; Plasticity Induced Crack Closure; Bauschinger Effect; Strain Hardening

---

## 1. Introduction

The adaption of lightweight construction from aerospace to automotive is one of the most promising approaches for energy efficiency in transporting systems. An accompanying phenomenon is fatigue damage, as one of the most probable failure mechanisms in aerospace components. Accordingly, to obtain a damage tolerant design and structural integrity there is a necessity of prediction of fatigue crack growth and the corresponding failure. The Paris-law (Paris & Erdogan, 1963), a common empirical approach that describes fatigue crack growth, uses two parameters to link the fatigue crack growth rate to the applied stress intensity factor with a potential function. Unfortunately, this function only keeps its validity if the crack is subjected to constant amplitude loading (Alderliesten, 2015). In-service-loads usually consist of variable stress amplitudes, which cannot be described with this propagation law. The application of increased load amplitudes leads to transient crack growth behavior, a strong reduction of the fatigue crack growth rate (fcgr). One consequence of this overload (OL) effect is that lifetime prediction is hardly possible as the unique link of the empirical law loses its validity. The importance of this question has led to long time research, whereas in the last 10 years the focus was set to local stress and strain measurements (Croft, et al., 2012; Belnoue, et al., 2010; Steuwer, et al., 2010; Lopez-Crespo, et al., 2013) since these are the keys in understanding the underlying mechanisms.

### 1.1. Overload mechanisms

The mechanisms of the OL effect are discussed since more than 40 years. Possible mechanisms are: crack tip blunting, crack deflection, compressive residual stresses in front of the crack tip and plasticity induced crack closure (Sadananda, et al., 1999). Nowadays, researches focusses mainly on the last two. When OLs are applied, the increased stress intensity leads to an increase in the stress fields and thereby to an increase in plasticity in front of the crack tip. When the applied force is zero, the plastically deformed and thereby elongated material in the plastic zone induces compressive residual stresses. Although this process always occurs during fatigue (fig. 1a) and the crack always builds a cyclic plastic zone with stretched material while propagation, increased load amplitudes of OLs lead to a strong increment both in spatial dimension and in absolute value of these compressive RS (Ellyin & Wu, 1992). When the crack is loaded again at the former fatigue level, the compressive RS superimpose with the crack tip stress field and lead to a reduction in strain and thereby to a reduction in the cyclic plastic zone size and the driving force (i.e. crack tip opening displacement (CTOD), fig. 1d). Correspondingly, the damaging of the material is decreased and the crack is decelerated. After further crack growth in this region, a new surface is formed at the crack flanks in which the stressed material can relax. As a consequence, a geometric misfit of the crack flanks occurs which leads to contact before the external forces reach zero during unloading, the plasticity induced crack closure (PICC fig. 1b). Similar to the OL-compressive RS, this process always happens within the cyclic plastic zone, but the OL increases it. PICC leads to a reduction in the stress intensity factor  $K$ -range ( $\Delta K_{\text{eff}}$ ), because the crack can only damage the material at the stress intensity that opens it ( $K_{\text{OP}}$ ) when it is open (Elber, 1970). Although many experts in this field are confident about the dominance of PICC, there are both numerical (Ochensberger & Kolednik, 2016; Ellyin & Wu, 1992) and experimental evidences (Thielen, et al., 2016) that the compressive RS must not be neglected in a proper variable amplitude model.

## 1.2. Influence of hardening on crack tip driving force

Materials show a different sensitivity regarding the OL-effect. There are materials with a strong reaction, others with less (Skorupa, 1998). A possible explanation is the different hardening behavior. Strain hardening is known to have a strong effect on the  $CTOD$  (Shih, 1981), therefore it seems to be obvious that it also plays an important role, when changes in the opening behavior lead to transient effects. Pommier and Bompard showed in an extensive numerical study (Pommier, 2001; Pommier & Bompard, 2000) that cyclic strain hardening behavior causes a rotation of the plastic zone in direction of the crack flanks behind the tip. They postulate that due to the hardening, the energy that is needed to form a plastic zone at the prior location is increased and the material becomes more resistant against deformation in this region. As a consequence, the required opening stress is increased since those RS that lead to PICC concentrate at the process zone.

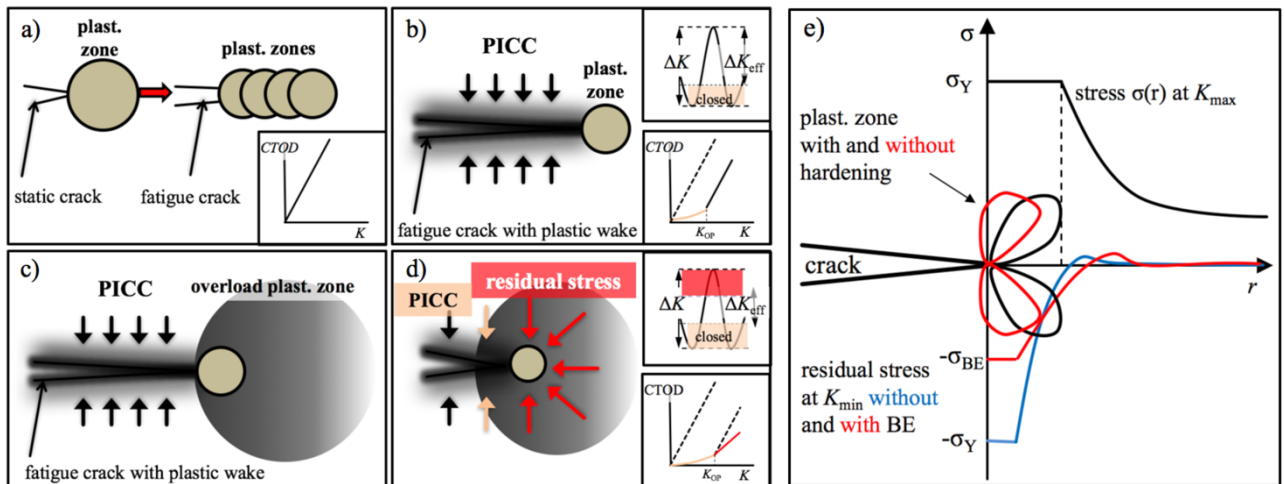


Fig. 1. a-d) (Thielen, et al., 2016) Generation of crack tip shielding mechanisms: a) Without shielding mechanisms, the answer of the driving force (i.e.  $CTOD$ ) to applied  $K$  is linearly, continuously increasing. Crack opening causes a plastic zone, fatigue crack growth builds a continuous, cyclic plastic zone. b) The cyclic plastic zone causes a plastic stretch in the wake that leads to preliminary flank contact. As a consequence, the answer of the driving force on applied  $K$  is delayed and thereby reduced. c) OLs cause a larger plastic zone with increased effects on the crack: d) after OL, PICC and  $K_{op}$  is increased. Furthermore, RS are generated in the  $K$ -dominated region. In contradiction to PICC, they directly reduce crack tip strain fields which has an effect on the whole opening cycle and thereby reduces the slope of the driving force. e) Influence of hardening mechanisms on crack tip behavior by the example of plastic zone with and without hardening and the stress/RS distribution as a function of the BE. Strain hardening leads to a rotation of the plastic zone to the flanks. The stress concentration increases the amount of PICC. The BE reduces the maximum possible compressive RS, which leads to a decrease in relaxation and thereby to a decreased PICC.

After tensile plastification, one can observe a reduction of the yield stress when the sign of the applied load is changed in many materials. This Bauschinger effect (BE), is caused by the superposition of stresses with RS. An explanation of the interplay of the BE with OL effects requires a prior separation of RS effects. According to (Macherauch, et al., 1973), RS can be separated into macro- and micro RS. While macro RS (1st kind) are constant over several grains, micro RS (2nd kind) change from grain to grain or even from regions with high dislocation density to those with low inside one grain (3rd kind). Locally, micro RS are always in equilibrium and thereby hard to measure. The yield stress at load reversal is reduced since grains with compressive micro RS have a reduced elastic region in compression.

The complex impact of the BE on OL mechanisms is shown in as well in figure 1e). Under load ( $K_{max}$ ), the stresses cannot exceed the materials' yield stress which can be seen in their distribution (black curve). When the external load is removed ( $K_{min}$ ), a reversed plastic zone with compressive residual stresses is formed (blue curve), even if no external compressive stresses are applied. At this zone, the stresses cannot be above the yield stress in compression. If this stress is exceeded, the material begins to flow again which leads to a relaxation of RS and thereby to the reduction in shielding mechanisms. Without BE, this stress is almost similar to the tensile yield stress

for most metals. For materials that show a BE, the back stress of micro RS prevents this. Accordingly, due to the strong plastification at the crack tip, the resulting macro RSs cannot reach the prior compressive yield stress anymore, just a reduced Bauschinger yield stress. This is detrimental for PICC since this effect is based on a relaxation effect that can only occur from stresses that are not in local equilibrium (1st kind RS). As a consequence, the BE reduces the possible relaxation and thereby PICC.

The impact of BE on RS shielding is different since this effect is not based on relaxation of 1st kind RS but on superposition of crack tip stresses with RS. The important point is that the superposition occurs locally with micro RS (2nd/3rd kind). These RSs distribute, according to the Masing model (Masing, 1923), the following: when applying tensile stresses, plastic flow begins in soft grains (or phases) first, so they become into the compressive state at load withdrawal while strong grains remain in tensile RS to obtain local equilibrium. When tensile stress is applied again, the BE acts in a way that strengthens soft grains and weakens hard grains. Accordingly, the plastic flow is still hindered in soft grains, which are detrimental to yielding, due to the local micro RS state. Consequently, the crack tip shielding effect of RS is still active. Summarizing, one can expect that although BE directly affects the macro RS state, the influence on the prevented strain after an OL in front of the crack tip due to the RS effect is not distinct.

The hereby presented mechanisms are not integrated in the common approaches of variable amplitude fcgr predictions. The consequences for the stress concentration, as well as experimental evidence of this, has not been investigated, yet.

## 2. Experiment and Discussions

Investigating the OL effect's mechanisms requires the knowledge of local displacements, stresses and strains. To achieve this, two techniques have been used. The magnetic Barkhausen noise (MBN) is one of the few methods that allows the measurement of local stresses in a scanning technique. MBN is based on the correlation of the direction of the magnetic domains with the local stress state (Boller, et al., 2011). It was used to quantify the distribution of RS and how they are influenced by different OL levels and during further cycling. The digital image correlation (DIC) as second technique has become standard to obtain strains and displacement fields with optical systems. Electron beam stability of modern SEMs opened the possibility to use DIC at high spatial resolution of several nm pixel size when regarding several error sources (Kammers & Daly, 2013) in careful experiments. These fields can be used to quantify the plastic zone size and shape and the crack tip driving force.

### 2.1. Material and fatigue parameters

The material S960Q used in this study is a high strength low alloy steel, further described in (Thielen, et al., 2016). It behaves nearly ideal plastically (yield stress  $\sigma_Y = 1,010$  MPa, tensile strength  $\sigma_{UTS} = 1,050$  MPa, strain hardening exponent  $n \approx 100$ ) with a strong BE: after plastification, approx. 30% of  $\sigma_Y$  can be reached. These properties allow us to use it as reference material regarding the plastic zone behavior according to Fig. 1.

Fatigue tests were conducted at four single edge notch tensile-samples that were notched for 0.2 mm by spark erosion. Crack initiation was performed at  $R = -1$ , further crack growth at  $R = 0$  at a constant stress amplitude of  $\sigma_{max} = 300$  MPa. The crack length was measured using replica technique, the propagation rate was evaluated using the ASTM-E647 standard.

### 2.2. Methods and results

In the first part of the experiment, the influence of the OL level on RS and fcgr was investigated. Points of interest were the determination if there was a saturation in RS or in the OL effect on transient crack growth. Therefore, three cracks have been fatigued under constant load amplitude conditions. After reaching a defined length of 750  $\mu\text{m}$  (equal to  $K_{max} = 20$  MPa $\sqrt{\text{m}}$ ), three different OL ratios have been applied:  $OL_1 = 50\%$ ,  $OL_2 = 100\%$  and  $OL_3 = 150\%$  (additional stress). After a RS measurement, the transient fatigue crack growth was investigated (fig. 2a).

The RS measurement was performed with a Barkhausen noise and eddy current microscope (BEMI), the calibration of the device is described in detail by (Sheikh-Amiri, et al., 2014; Thielen, et al., 2016). The RS distribution was obtained at an area of  $2 \times 2 \text{ mm}^2$  with a spatial resolution of approx.  $10 \text{ }\mu\text{m}$ . The kind of RS that are measured depends on the local microstructure. The hereby used steel has a fine microstructure, so at every measurement point, several grains are averaged and 1st kind RS are measured. The results are shown in fig. 2b).

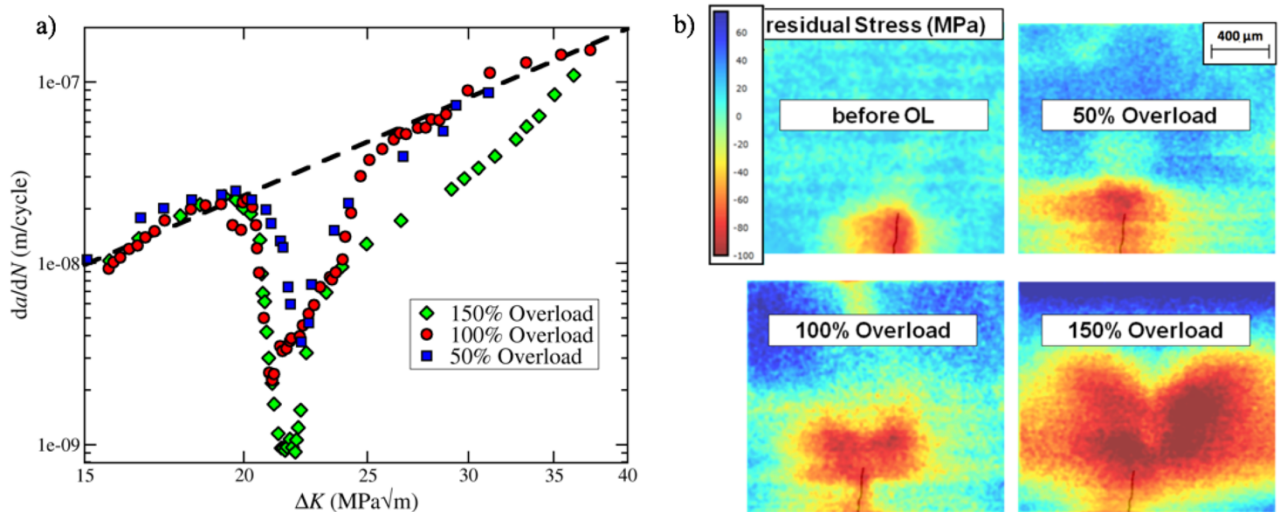


Fig. 2. a) Transient crack growth speed after OL differing from the linear Paris behavior under constant force amplitude loading. At  $K = 20 \text{ MPa}\sqrt{\text{m}}$  different OLs have been applied. Higher OLs lead to stronger deceleration over a longer period. b) Influence of OL level on RS distribution, measured with MBN, the crack position in the image was overlain in post processing. Before the OL, the surrounding closure stresses are visible. Applying and OL increases the stress field. Higher OL lead to higher compressive RS in amplitude as well as in a wider spatial distribution.

Our measurements indicate that the crack is always surrounded by compressive residual stresses. Before the overload, these stresses distribute locally at the crack flanks, hardly in front of the crack. One can suggest them being closure stresses of the cyclic plastic zone. After applying different OL levels, compressive residual stresses in front of the crack tip become visible. An increment of the OL level leads to stronger RS fields, both in maximum compressive residual stress and in spatial distribution. The distribution of RS fields correlates with the crack growth curves. Correspondingly, the minimum  $fcgr$  decreases with increasing OL level, the crack length to overcome the OL region and consequently the number of cycles in the retardation region increases. After passing the OL region, the Paris line is reached again. Although the lowest stresses cannot be seen in the images since the scale has been chosen in a way the gradient is shown and not the lowest stress, the measured compressive RS seems to saturate much below the yield stress. The maximum compressive stresses that were measured are  $-95 \text{ MPa}$  before OL,  $-108 \text{ MPa}$  at 50% OL,  $-125 \text{ MPa}$  at 100% OL and  $-127 \text{ MPa}$  at 150% OL. Possible reasons for this could be a gradient which is steeper than the spatial resolution of BEMI, or a saturation because of the BE.

Changes of the plastic zone and the crack tip driving force have been evaluated using SEM-based DIC. Common characterization techniques for the driving force are based on the crack tip opening displacement, the  $K$  and the  $J$ -integral. In this study, the  $CTOD$  and the local  $J$ -integral were used.

The images were collected with Zeiss Sigma VP FE-SEM and secondary electrons at 500 pA current to keep the beam drift as low as possible. An *in situ* tensile tester type Kammrath & Weiss 10kN was used, the force was increased in 10 steps from 0 MPa to 300 MPa, the level of the fatigue tests. The field of view for the  $J$ -Integral was  $115 \times 85 \text{ }\mu\text{m}^2$  with  $3,072 \times 2,304$  pixels, so the corresponding pixel size was approx.  $37 \text{ nm}$ . The  $CTOD$  was evaluated at the crack tip with a field of view of  $13 \times 10 \text{ }\mu\text{m}^2$  with  $1,024 \times 768$  pixels at a pixel size of  $12.4 \text{ nm}$ . The images to reveal the plastic zone size had a larger field of view of  $440 \times 330 \text{ }\mu\text{m}^2$  to obtain the whole plastic zone.

The pixel resolution was 3,072 x 2,304 pixels, the corresponding size was 140 nm. The DIC evaluation was performed with the software VEDDAC and a pixel pitch of 20 x 20 pix. with a measurement field of 50% overlap, which leads to approx. 17700 displacement vectors per image (15 x 15 pix and 3500 vectors for *CTOD*). To evaluate the plastic zones, the images have been smoothed using a Gaussian filter. The driving forces *CTOD* and *J*-Integral images were kept unsmoothed since local resolution must not be decreased and the underlying displacements are quite large and thereby less sensitive to measurement noise.

The *CTOD* was calculated by subtracting the displacement lines of the crack flanks (Thielen, et al., 2016). In order to decrease the influence of local errors but still keep the high locality of the crack tip, the *CTOD* has been calculated as mean value of the first micrometer behind the crack tip mean *CTOD*.

The *J*-integral was evaluated in analogy to (Vavrik & Jandajsek, 2014) but with two differences. First, we used SEM-based DIC as input parameter for the calculation. Second, strain fields were calculated from the DIC software and the plastic zone behavior was obtained from these results, not from further measurements since the plasticity was restricted to the plastic zone.

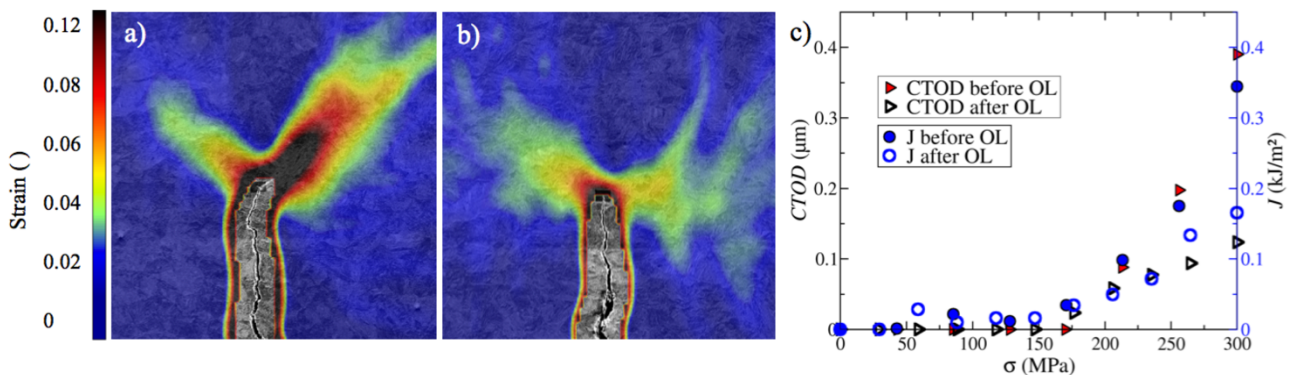


Fig. 3. a) Strain field in front of the crack tip at fatigue stress before the OL. The plastic zone corresponds to the yellow strains. DIC results have been overlain to the corresponding SEM image at this stress. b) The same measurement with the crack at maximum retardation after a 100% OL. A decrement of size and strain amplitude is visible, as well as a rotation of the strain field. c) Crack tip driving force, characterized by *CTOD* and *J*-Integral as a function of applied stress and the OL effect. Before the OL, a delayed opening of 50% is visible, reducing the maximum driving force. This opening level does not change much after the OL, but the slope of driving force increment is decreased, indicating the dominating influence of RS in front of the crack tip.

Figure 3 shows the strain fields before the OL (a) and after the application of the 100%-OL at maximum retardation (b). Before OL, the strains concentrate in approx. 45° to the crack plane with an asymmetry to the right side which might be due to the local crack orientation. After the OL, a decrement of strain distribution is visible indicating the decrement in the crack tip driving force. Furthermore, the orientation changed to nearly 90° in respect to the crack plane, a behavior that is expected to occur at strain hardening (Fig. 1b)). Since the used material hardly shows any hardening, this indicates that the RS fields acts in a comparable way at the strain fields. Fig. 3c) shows the change of the crack tip driving force, indicated by *CTOD* and *J*-Integral as a function of the applied force before the OL and the max. retardation position. The comparison of both driving forces agrees well with the prediction of Shih (Shih, 1981), from which 1 kJ/m² in *J* corresponds to 1 μm of *CTOD* for this material. A delayed opening and thereby a reduction in the driving force is visible for both crack position but it hardly changes after the OL. A decrement of the maximum driving force after this OL is achieved by a reduction of the slope. This indicates a dominance of the RS mechanism at this crack tip position, since they superimpose at the whole opening cycle.

### 3. Conclusions and Outlook

Possible parameters influencing the correlation of materials' fatigue properties with OL behavior have been discussed. Strain hardening is expected to rotate the plastic zone to the crack flanks and thereby increase PICC. The BE is expected to restrict the possible compressive residual stresses (1st kind) and thereby reduce PICC. For the

proper identification of their interplay with OL mechanisms, the determination of local stress, strain and displacement fields is mandatory. With two methods that have been applied to a model material we showed that:

- The determination of local RS fields after OLs is possible with a calibrated MBN microscope.
- RS fields show a correlation with corresponding transient fcgr curves.
- Saturation of the RS at a level much below the yield stress was observed and needs to be verified with other measurement techniques and other materials to determine if it is a consequence of BE or a measurement artefact.
- Displacement, strain and stress fields could be achieved from DIC measurements
- Changes in plastic zone size was observed after the overload. A decrement of size and strains and changes of the shape have been measured. The behavior indices, that macro RS lead to comparable effects as strain hardening.
- The experimental local *CTOD*- and *J*-Integral-values, calculated from DIC-measurements, are in accordance to the crack tip driving force. They show consistent behavior regarding the delayed crack opening and maximum driving force.
- A decrement of the maximum driving force at the maximum retardation after OL application was measured, however it was achieved by a reduced slope (RS dominance) and not by a change in first opening (PICC dominance). The change of this behavior inside the OL region will be investigated in further studies in detail.

We showed, that the measurement of main effects that possibly influence OL mechanisms is possible. Next studies will be performed with the same experiments on materials that show distinct strain hardening to compare the behavior to this ideal plastic material. The focus will be set on the saturation of RS, the plastic zone rotation, that was already visible due to the compressive RS and the change of the opening behavior in respect to crack position inside the OL region.

## Acknowledgements

We thank the Fraunhofer Institute of Non-Destructive Testing for the permission of using of BEMI.

We also thank the Deutsche Forschungsgemeinschaft DFG for funding the project under grant MA3322/6-1.

## References

- Alderliesten, R. C., 2015. How proper similitude can improve our understanding of crack closure and plasticity in fatigue. *International Journal of Fatigue*.
- Belnoue, J. P. et al., 2010. Evaluation of the overload effect on fatigue crack growth with the help of synchrotron XRD strain mapping. *Engineering Fracture Mechanics*, 77(16), pp. 3216-3226.
- Bichler, C. & Pippan, R., 2007. Effect of single overloads in ductile metals: A reconsideration. *Engineering Fracture Mechanics*, 75(8), pp. 1344-1359.
- Boller, C. et al., 2011. Electromagnetism as a means for understanding materials mechanics phenomena in magnetic materials. *Materialwissenschaft und Werkstofftechnik*, 42(4), pp. 269-278.
- Croft, M. et al., 2012. Fatigue crack growth "overload effect": mechanistic insights from in-situ synchrotron measurements. *The Journal of Strain Analysis for Engineering Design*, 47(2), pp. 83-94.
- Elber, W., 1970. Fatigue crack closure under cyclic tension. *Engineering Fracture Mechanics*, 2(1), pp. 37-45.
- Ellyin, F. & Wu, J., 1992. Elastic-plastic analysis of a propagating crack under cyclic loading. *International Journal of Fracture*, Volume 56, pp. 189-208.
- Kammers, A. D. & Daly, S., 2013. Digital Image Correlation under Scanning Electron Microscopy: Methodology and Validation. *Experimental Mechanics*, 53(9), pp. 1743-1761.
- Lopez-Crespo, P. et al., 2013. Overload effects on fatigue crack-tip fields under plane stress conditions: surface and bulk analysis. *Fatigue & Fracture of Engineering Materials & Structures*, 36(1), pp. 75-84.
- Macherauch, E., Wohlfahrt, H. & Wolfstieg, U., 1973. Zur zweckmaessigen Definition von Eigenspannungen. *HTM*, 28(3), pp. 201-211.
- Masing, G., 1923. Zur Heyn'schen Theorie der Verfestigung der Metalle durch verborgen elastische Spannungen. In: S. B. Heidelberg, ed. *Wissenschaftliche Veröffentlichungen aus dem Siemens-Konzern*. Berlin: Springer Berlin Heidelberg, pp. 231-239.
- Meggiolaro, M., 2003. On the dominant role of crack closure on fatigue crack growth modeling. *International Journal of Fatigue*, 25(9-11), pp. 843-854.
- Ochensberger, W. & Kolednik, O., 2016. Overload effect revisited - Investigation by use of configurational forces. 83(2), pp. 161-173.
- Paris, P. C. & Erdogan, F., 1963. A critical analysis of crack propagation laws. *Journal of Fluids Engineering*, 85(4), pp. 528-533.
- Pommier, S., 2001. Plane strain crack closure cyclic hardening. *Engineering Fracture Mechanics*, 69(1), pp. 25-44.

- Pommier, S. & Bompard, P., 2000. Bauschinger effect of alloys and plasticity-induced crack closure: A finite element analysis. *Fatigue and Fracture of Engineering Materials and Structures*, 23(3), pp. 129-139.
- Sadananda, K., Vasudevan, A. K., Holtz, R. L. & Lee, E. U., 1999. Analysis of overload effects and related phenomena. *International Journal of Fatigue*, Volume 21, pp. 233-246.
- Sheikh-Amiri, M. et al., 2014. On the role of crystal and stress anisotropy in magnetic Barkhausen noise. *Journal of Magnetism and Magnetic Materials*, Volume 372, pp. 16-22.
- Shih, C., 1981. Relationships between the J-integral and the crack opening displacement for stationary and extending cracks. *Journal of the Mechanics and Physics of Solids*, 29(4), pp. 305-326.
- Skorupa, M., 1998. Load Interaction Effects During Fatigue Crack Growth Under Variable Amplitude Loading — a Literature Review . Part I : Empirical Trends. *Fatigue & Fracture of Engineering Materials & Structures*, Volume 21, pp. 987-1006.
- Steuer, A. et al., 2010. The evolution of crack-tip stresses during a fatigue overload event. *Acta Materialia*, 58(11), pp. 4039-4052.
- Thielen, M. et al., 2016. Using Barkhausen Noise and Digital Image Correlation to Investigate the Influence of Local Residual Stresses on Fatigue Crack Propagation. *Materials Performance and Characterization*, 5(3).
- Vavrik, D. & Jandjsek, I., 2014. Experimental evaluation of contour J integral and energy dissipated in the fracture process zone. *Engineering Fracture Mechanics*, Volume 129, pp. 14-25.